

Structure and function of Zucchini endoribonuclease in piRNA biogenesis

Hiroshi Nishimasu^{1*}, Hirotsugu Ishizu^{1,2*}, Kuniaki Saito², Satoshi Fukuhara¹, Miharuru K. Kamatani², Luc Bonnefond^{1†}, Naoki Matsumoto¹, Tomohiro Nishizawa¹, Keita Nakanaga³, Junken Aoki³, Ryuichiro Ishitani¹, Haruhiko Siomi², Mikiko C. Siomi^{1,2,4} & Osamu Nureki^{1,4}

PIWI-interacting RNAs (piRNAs) silence transposons to maintain genome integrity in animal germ lines^{1–4}. piRNAs are classified as primary and secondary piRNAs, depending on their biogenesis machinery^{5–10}. Primary piRNAs are processed from long non-coding RNA precursors transcribed from piRNA clusters in the genome through the primary processing pathway^{5,8–10}. Although the existence of a ribonuclease participating in this pathway has been predicted, its molecular identity remained unknown. Here we show that Zucchini (Zuc), a mitochondrial phospholipase D (PLD) superfamily member¹¹, is an endoribonuclease essential for primary piRNA biogenesis. We solved the crystal structure of *Drosophila melanogaster* Zuc (DmZuc) at 1.75 Å resolution. The structure revealed that DmZuc has a positively charged, narrow catalytic groove at the dimer interface, which could accommodate a single-stranded, but not a double-stranded, RNA. DmZuc and the mouse homologue MmZuc (also known as Pld6 and MitoPLD)^{12–14} showed endoribonuclease activity for single-stranded RNAs *in vitro*. The RNA cleavage products bear a 5'-monophosphate group, a hallmark of mature piRNAs. Mutational analyses revealed that the conserved active-site residues of DmZuc are critical for the ribonuclease activity *in vitro*, and for piRNA maturation and transposon silencing *in vivo*. We propose a model for piRNA biogenesis in animal germ lines, in which the Zuc endoribonuclease has a key role in primary piRNA maturation.

Zuc is conserved among animals, and loss-of-function mutations in *zuc* in flies and mice cause a severe defect in piRNA accumulation in the germ lines, implying a role for Zuc in piRNA biogenesis^{8,10,11,13,15,16}. Zuc contains a mitochondrial localization sequence (MLS) at the amino terminus and an HKD (His-Lys-Asp) motif, a hallmark of PLD superfamily members, in the central region (Supplementary Fig. 1a)¹². The PLD superfamily members have diverse cellular functions¹⁷, and Zuc shares the highest sequence similarity with the bacterial nuclease Nuc^{18,19} among the superfamily members (Supplementary Fig. 1b). Zuc has therefore been considered to be a candidate for the RNase required for piRNA biogenesis¹¹. However, previous attempts to detect the nuclease activity in Zuc were unsuccessful^{12,13}.

To obtain structural clues to Zuc's function, we solved the 1.75-Å resolution crystal structure of the cytoplasmic region (residues 41–253) of DmZuc, which lacks the N-terminal MLS and a predicted transmembrane helix (Fig. 1a and Supplementary Fig. 2a–c). The structure consists of a catalytic domain (residues 49–62 and 89–245) and a zinc-binding domain (residues 63–88), with the two protomers in the asymmetric unit forming a dimer. Co-immunoprecipitation experiments suggested this oligomeric state *in vivo* (Supplementary Fig. 2d). The catalytic domain consists of an eight-stranded mixed β -sheet flanked by α -helices on both sides, and shares structural similarity with the catalytic domains of other PLD superfamily members, such as Nuc^{19,20} (PDB 1BYR; 26% sequence identity, root mean

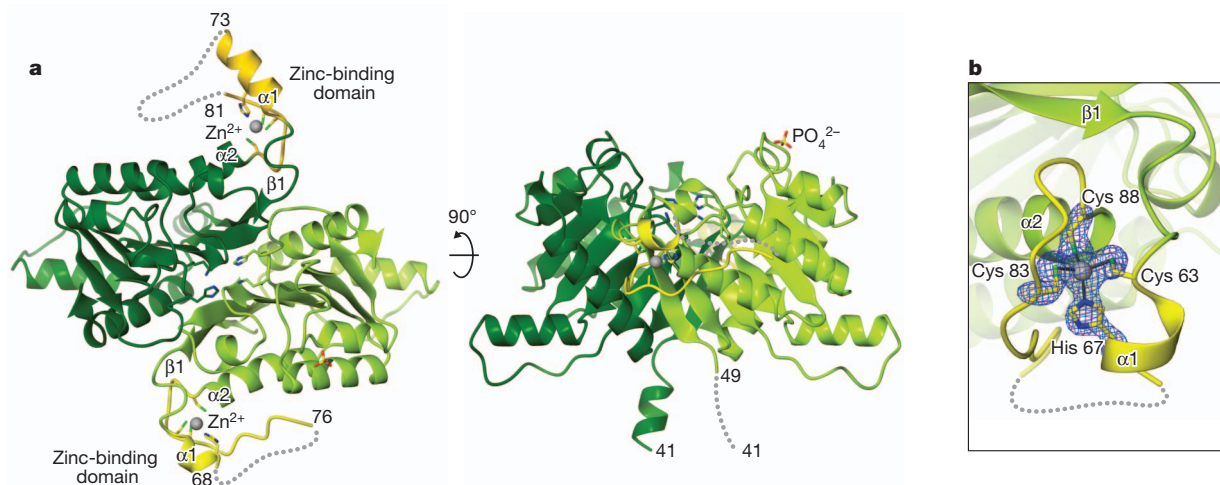


Figure 1 | Crystal structure of DmZuc. **a**, Overall structure. The two protomers are coloured green and yellow-green, and the zinc-binding domains are coloured gold and yellow. The bound zinc ions are shown as grey spheres. Cys 63, His 67, Cys 83, Cys 88, His 169, Lys 171 and the bound phosphate ion

are shown as sticks. Disordered regions are shown as dashed lines. **b**, The zinc-binding domain. The bound zinc ion is shown as a grey sphere, and a simulated annealing $F_o - F_c$ omit electron density map (contoured at 4σ) is shown as a blue mesh.

¹Department of Biophysics and Biochemistry, Graduate School of Science, The University of Tokyo, Tokyo 113-0032, Japan. ²Department of Molecular Biology, Keio University School of Medicine, Tokyo 160-8582, Japan. ³Graduate School of Pharmaceutical Sciences, Tohoku University, Miyagi 980-8578, Japan. ⁴Japan Science and Technology Agency (JST), Core Research for Evolutional Science and Technology (CREST), Saitama 332-0012, Japan. †Present address: Institut de Génétique et de Biologie Moléculaire et Cellulaire, UMR7104 CNRS-UDS, INSERM U964, 1 rue Laurent Fries, BP 10142, 67404 Illkirch Cedex, France.

*These authors contributed equally to this work.

squared deviation 1.8 Å for 145 C α atoms) (Supplementary Fig. 3a, b). His 169 and Lys 171 in the HKD motif in the two protomers form an active site at the dimer interface, and Asp 176 in the motif helps to maintain the structural integrity of each protomer (Supplementary Fig. 2e). The crystal structure revealed that a zinc ion is tetrahedrally coordinated by Cys 63, His 67, Cys 83 and Cys 88 in the zinc-binding domain, which is mostly disordered, and is absent from the other PLD superfamily members (Fig. 1b and Supplementary Fig. 4a, b). In the CHCC motif, only Cys 83 is conserved in animals (Supplementary Fig. 1a). In the corresponding region of MmZuc, the residues Cys 49, Glu 51, Cys 66 and Cys 68 are highly conserved among animals except for flies (Supplementary Fig. 1a), suggesting that these residues may coordinate a zinc ion in these species.

The active-site groove is composed of conserved residues from the two protomers, including Tyr 112, His 169, Lys 171, Ser 204, Asn 206, Trp 207, Thr 208, Asn 215 and Glu 217, which correspond to Tyr 35, His 94, Lys 96, Ser 109, Asn 111, Phe 112, Thr 113, Asn 120 and Glu 122, respectively, in Nuc (Fig. 2). Nuc cleaves substrates through a two-step catalytic mechanism, in which His 94 in one protomer forms a phosphoenzyme intermediate with a substrate phosphorus atom, followed by the hydrolysis of this intermediate by a water molecule, activated by His 94 in the other protomer^{19,21}. Lys 96, Ser 109, Asn 111 and Glu 122 in Nuc form a hydrogen-bonding network and participate in catalysis¹⁹. The active-site residues are similarly arranged in DmZuc and Nuc (Fig. 2b, c and Supplementary Fig. 3c), suggesting that Zuc cleaves a substrate phosphodiester linkage through a similar catalytic mechanism. However, a structural comparison revealed a notable difference in their active-site architectures (Fig. 2a and Supplementary Fig. 5a, b). Nuc cleaves single-stranded and double-stranded nucleic acids *in vitro*^{18,22} (Supplementary Fig. 6), and has a wide, positively charged groove that can readily accommodate double-stranded nucleic acids¹⁹ (Supplementary Fig. 5a). In contrast, the active-site groove of DmZuc is narrower than that of Nuc, and can apparently accommodate single-stranded, but not double-stranded, nucleic acids (Fig. 2a and Supplementary Fig. 5b). This structural difference is partly due to the replacements of Gly 64 and Ala 115 in Nuc with the bulkier Met 141 and Leu 210 residues in DmZuc, respectively (Fig. 2a, b and Supplementary Fig. 3c). A phosphate ion derived from

the crystallization buffer binds to a positively charged patch near the active-site groove (Supplementary Fig. 5c), suggesting that this patch could interact with the phosphate group of nucleic acid substrates. The molecular surface on the side opposite the active-site groove is positively charged (Supplementary Fig. 5d). The N termini of the two protomers are located on the same face, and the N-terminal residues 41–48 of one protomer form a positively charged helix, which would follow the transmembrane helix (residues 41–48 are disordered in the other protomer). This structural feature supports a previous model in which Zuc localizes on the outer mitochondrial membrane^{12–15}. Taken together, the structural features of DmZuc suggested that Zuc is a single-stranded nuclease that functions on the mitochondrial surface.

To determine whether DmZuc is a nuclease, purified DmZuc (residues 41–253; hereafter referred to as wild-type (WT) DmZuc) was incubated with a 42-nucleotide (nt) single-stranded RNA (ssRNA) labelled with ³²P at the 5' end. DmZuc cleaved the ssRNA substrate (Fig. 3a). In contrast, the DmZuc mutants H169A, K171A, N206A and N215A failed to cleave the substrate (Fig. 3a), highlighting the importance of the conserved residues for the ssRNase activity. These results also confirmed that the observed cleavage was not due to contaminants. A DmZuc Δ 63–88 mutant, lacking the zinc-binding domain, showed decreased ssRNase activity (Fig. 3a), indicating the importance of this domain for the nuclease activity. The crystal structure of a shorter DmZuc construct (residues 89–250), lacking the β 1 strand that contributes to dimerization, was solved as a monomer (Supplementary Fig. 2b). This shorter construct failed to cleave the ssRNA substrate (Fig. 3a), indicating the requirement of dimerization for the ssRNase activity. Purified MmZuc (residues 35–221) also showed a ssRNase activity comparable to that of DmZuc (Fig. 3a). Thus, Zuc is an evolutionarily conserved RNase. Unlike Nuc (Supplementary Fig. 6), DmZuc cleaved poly(U) and circular ssRNA, and also ssDNA (Supplementary Fig. 7a), but not double-stranded RNA (dsRNA) (Fig. 3b). Thus, DmZuc is a single-strand-specific endonuclease. Although the poly(U) cleavage products showed an even distribution, DmZuc did not always cleave the ssRNA substrates at specific nucleotides (Fig. 3b), suggesting that DmZuc does not have strict sequence specificity. DmZuc showed similar activity in the presence of magnesium ions or EDTA (Fig. 3c), indicating that, like Nuc^{19,22}, DmZuc is a metal-independent nuclease. The DmZuc ssRNase activity was inhibited by NaCl at concentrations of 50 mM or higher (Fig. 3c). Sodium ions may inhibit substrate binding, as observed for T4 DNA ligase²³ and the dsRNA-specific RNase Pac1 (ref. 24). We characterized the 5' end structure of the cleavage products, using the 42-nt ssRNA labelled with ³²P at the 3' end. The cleavage products showed resistance to treatment with 5'-phosphate ssRNA-specific exonuclease (Terminator Exonuclease) after treatment with calf intestinal phosphatase (Fig. 3d), suggesting that the cleavage products contain a 5' monophosphate. The endonuclease activity of DmZuc is modest *in vitro*, although it showed dose dependence (Supplementary Fig. 7b). The DmZuc activity may be stimulated *in vivo* by unknown cofactors. Although MmZuc reportedly hydrolysed the mitochondrial lipid cardiolipin to phosphatidic acid¹², the active-site groove of DmZuc seems too narrow to accommodate such a bulky lipid molecule as a substrate (Fig. 2a and Supplementary Fig. 5b). Indeed, neither DmZuc nor MmZuc hydrolysed cardiolipin *in vitro* (Supplementary Fig. 8). The reason for this discrepancy is currently unclear. Together, these results indicated that Zuc is an endonuclease specific for single-stranded nucleic acids.

To explore the biological relevance of the DmZuc ssRNase activity in transposon silencing, we expressed RNA-mediated interference (RNAi)-resistant WT and mutants of full-length DmZuc (residues 1–253) in DmZuc-depleted ovarian somatic cells (OSCs), and then monitored the expression levels of the *mdg1* transposon by quantitative PCR with reverse transcription (RT-PCR). Western blotting confirmed the similar expression levels of DmZuc WT and mutants (Fig. 4a). WT DmZuc rescued *mdg1* derepression, whereas the H169A and K171A mutants failed to rescue it (Fig. 4a). The *mdg1*

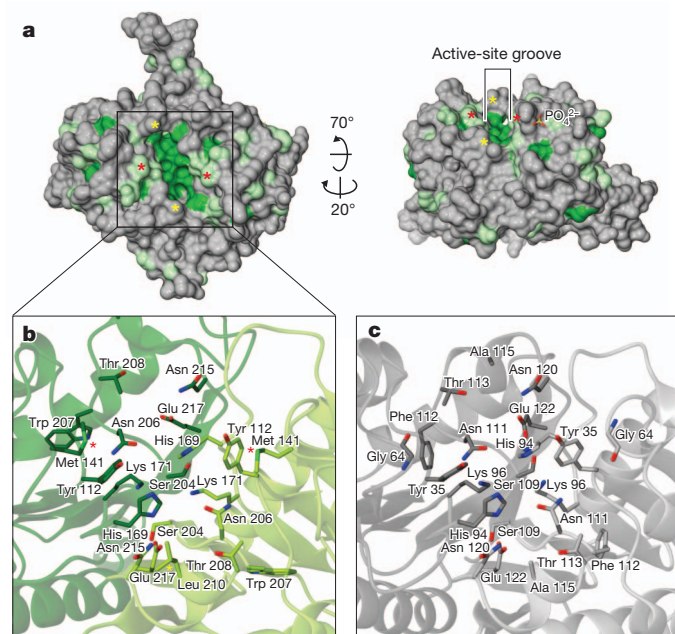


Figure 2 | Active site of DmZuc. **a**, Molecular surface of DmZuc. Conserved residues are coloured green, and Met 141 and Leu 210 are indicated by red and yellow asterisks, respectively. **b**, Active site of DmZuc. **c**, Active site of Nuc (PDB 1BYR).

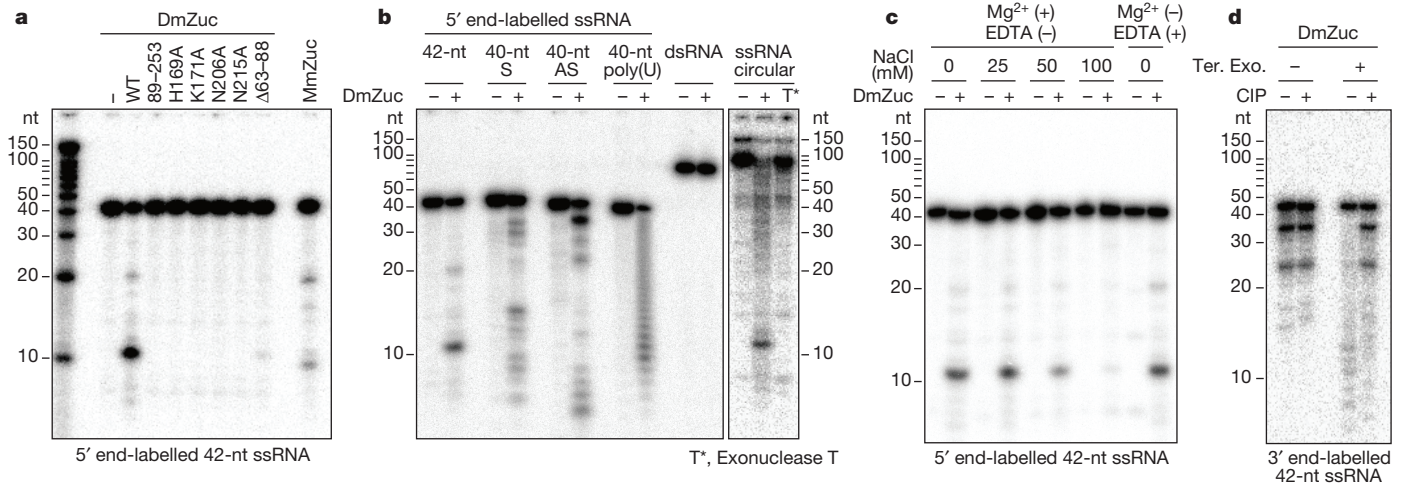


Figure 3 | Zuc is an endonuclease for single-stranded nucleic acids. **a**, DmZuc and MmZuc, but not monomeric DmZuc or the DmZuc mutants, cleave a 42-nt ssRNA substrate. **b**, DmZuc cleaves ssRNAs of various sequences and circular ssRNA, but not dsRNA. Exonuclease T failed to cleave the circular ssRNA. S and AS correspond to the sense and antisense strands of dsRNA, respectively. **c**, DmZuc endonuclease activity requires no magnesium ions, and is inhibited by NaCl. **d**, The ssRNA products cleaved by DmZuc have a 5' monophosphate. The cleavage products were resistant to treatment with Terminator Exonuclease (Ter. Exo.) after treatment with calf intestinal phosphatase (CIP).

expression was higher in OSCs expressing the H169A or K171A mutant than in control OSCs. The mutants may have dominant-negative effects, although the underlying mechanism is unknown. The C63A, H67A and $\Delta 63-88$ mutants rescued *mdg1* derepression. The $\Delta 63-88$ mutant had a lower ssRNase activity (about 5% of the WT activity) (Fig. 3a), which may suffice for transposon silencing. None of the mutants Y112A, S204A, N206A, W207A, T208A, N215A or E217A rescued *mdg1* derepression (Fig. 4a). These residues are conserved (Supplementary Fig. 1a) and form the active-site groove (Fig. 2b). The N218A mutant rescued *mdg1* derepression (Fig. 4a). Asn 218 is buried within the protein, and thus would not contribute to substrate binding. The H169A, K171A, N206A and N215A mutants lacked ssRNase activity *in vitro* (Fig. 3a) and the ability to repress transposons *in vivo* (Fig. 4a), indicating that the DmZuc ssRNase activity is critical for transposon silencing. The expression of WT DmZuc, but not that of the H169A and K171A mutants, rescued the defects in *Idefix*-piRNA maturation in DmZuc-depleted OSCs (Fig. 4b), suggesting that the DmZuc ssRNase activity is required for

primary piRNA maturation. RT-PCR after immunoprecipitation of DmZuc from OSCs revealed that DmZuc interacts with the piRNA precursors in OSCs (Supplementary Fig. 9). Together, these results indicate that Zuc is an endoribonuclease essential for primary piRNA processing.

We propose a model for primary piRNA biogenesis in *Drosophila* OSCs (Supplementary Fig. 10). Mature piRNAs show a strong bias for 5' uridine (1-U)^{5,25}. DmZuc cleaved ssRNAs with little sequence specificity, to produce ssRNA fragments bearing a 5' monophosphate (Fig. 3b, d), a hallmark of mature piRNAs associated with Piwi, suggesting that DmZuc generates the 5' end of mature piRNAs. These observations suggested that DmZuc cleaves piRNA intermediates to generate the 5' end of mature piRNAs during the processing step, and that Piwi then preferentially binds 1-U piRNAs during the loading step. Our findings provide a starting point for explaining the molecular mechanism by which Zuc recognizes genuine piRNA intermediates to produce mature piRNAs, which in turn should shed light on the mechanism of primary piRNA biogenesis in animal germ lines.

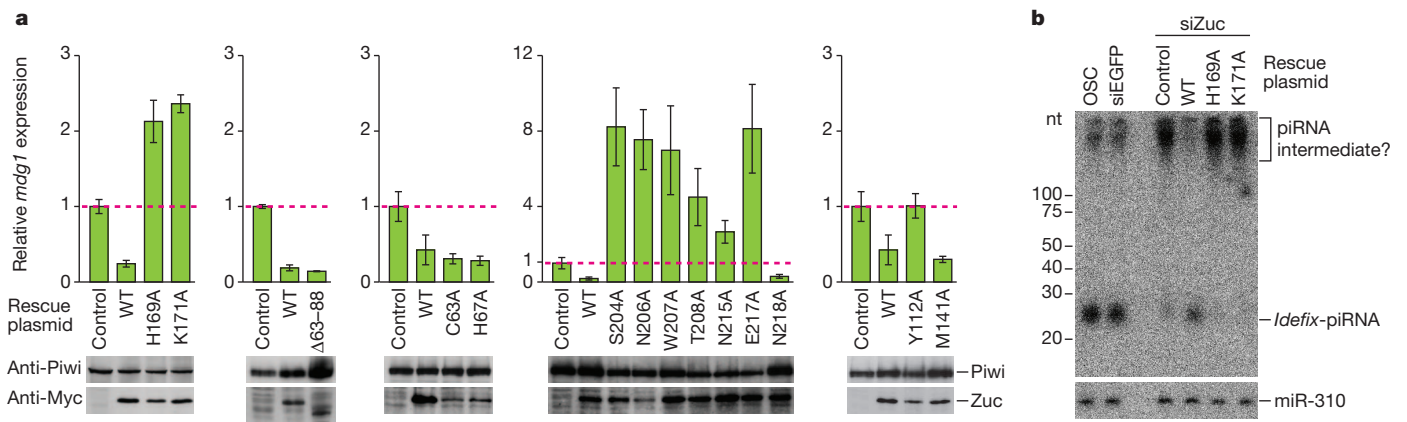


Figure 4 | DmZuc endoribonuclease activity is required for transposon silencing. **a**, Myc-tagged full-length WT and mutant DmZuc, mutated at a short interfering RNA (siRNA) recognition site and thus resistant to RNAi, were expressed in DmZuc-depleted OSCs. The expression levels of Piwi and DmZuc were examined by western blotting, and the expression levels of the *mdg1* transposon were monitored by quantitative RT-PCR. Results are shown as means \pm s.e.m. ($n = 3$). As a control, OSCs were transfected with an empty

vector. **b**, Northern blotting with a piRNA probe, *Idefix*-piR1-R, showed that WT DmZuc, but not H169A or K171A, rescued the defects in piRNA maturation in DmZuc-depleted OSCs. The expression of WT DmZuc increased mature piRNAs with a concomitant decrease in piRNA intermediate-like molecules. miR-310, one of the microRNAs in OSCs, was used as an internal loading control. 'piRNA intermediate?' corresponds to 'piRNA-intermediate-like molecules'.

METHODS SUMMARY

DmZuc and MmZuc were overexpressed in *Escherichia coli* as glutathione S-transferase (GST)-tagged proteins, and purified by glutathione-Sepharose, Resource S and Superdex 200 chromatography, as described²⁶. Crystals were obtained at 20 °C by the hanging-drop vapour diffusion method. X-ray diffraction data were collected on beamline BL32XU at SPring-8 (Hyogo, Japan). The crystal structure of DmZuc (residues 41–253) was determined by molecular replacement using the structure of monomeric DmZuc (residues 89–250), which was solved by the multiwavelength anomalous dispersion (MAD) method using a selenomethionine (SeMet)-labelled protein. Nuclease assays were performed in buffer containing 25 mM HEPES-KOH pH 7.4, 2.5 mM EDTA and 5 mM dithiothreitol. Rescue experiments were performed essentially as described previously¹⁵.

Full Methods and any associated references are available in the online version of the paper.

Received 29 May; accepted 14 August 2012.

Published online 14 October 2012.

- Malone, C. D. & Hannon, G. J. Small RNAs as guardians of the genome. *Cell* **136**, 656–668 (2009).
- Siomi, M. C., Sato, K., Pezic, C. & Aravin, A. A. PIWI-interacting small RNAs: the vanguard of genome defence. *Nature Rev. Mol. Cell Biol.* **12**, 246–258 (2011).
- Pillai, R. S. & Chuma, S. piRNAs and their involvement in male germline development in mice. *Dev. Growth Differ.* **54**, 78–92 (2012).
- Senti, K. A. & Brennecke, J. The piRNA pathway: a fly's perspective on the guardian of the genome. *Trends Genet.* **26**, 499–509 (2010).
- Brennecke, J. *et al.* Discrete small RNA-generating loci as master regulators of transposon activity in *Drosophila*. *Cell* **128**, 1089–1103 (2007).
- Vagin, V. V. *et al.* A distinct small RNA pathway silences selfish genetic elements in the germline. *Science* **313**, 320–324 (2006).
- Gunawardane, L. S. *et al.* A slicer-mediated mechanism for repeat-associated siRNA 5' end formation in *Drosophila*. *Science* **315**, 1587–1590 (2007).
- Malone, C. D. *et al.* Specialized piRNA pathways act in germline and somatic tissues of the *Drosophila* ovary. *Cell* **137**, 522–535 (2009).
- Li, C. *et al.* Collapse of germline piRNAs in the absence of Argonaute3 reveals somatic piRNAs in flies. *Cell* **137**, 509–521 (2009).
- Saito, K. *et al.* A regulatory circuit for piwi by the large Maf gene *traffic jam* in *Drosophila*. *Nature* **461**, 1296–1299 (2009).
- Pane, A., Wehr, K. & Schüpbach, T. *zucchini* and *squash* encode two putative nucleases required for rasiRNA production in the *Drosophila* germline. *Dev. Cell* **12**, 851–862 (2007).
- Choi, S. Y. *et al.* A common lipid links Mfn-mediated mitochondrial fusion and SNARE-regulated exocytosis. *Nature Cell Biol.* **8**, 1255–1262 (2006).
- Watanabe, T. *et al.* MITOPLD is a mitochondrial protein essential for nuage formation and piRNA biogenesis in the mouse germline. *Dev. Cell* **20**, 364–375 (2011).
- Huang, H. *et al.* piRNA-associated germline nuage formation and spermatogenesis require MitoPLD profusogenic mitochondrial-surface lipid signaling. *Dev. Cell* **20**, 376–387 (2011).
- Saito, K. *et al.* Roles for the Yb body components Armitage and Yb in primary piRNA biogenesis in *Drosophila*. *Genes Dev.* **24**, 2493–2498 (2010).
- Olivieri, D., Sykora, M. M., Sachidanandam, R., Mechtler, K. & Brennecke, J. An *in vivo* RNAi assay identifies major genetic and cellular requirements for primary piRNA biogenesis in *Drosophila*. *EMBO J.* **29**, 3301–3317 (2010).
- Ponting, C. P. & Kerr, I. D. A novel family of phospholipase D homologues that includes phospholipid synthases and putative endonucleases: Identification of duplicated repeats and potential active site residues. *Protein Sci.* **5**, 914–922 (1996).
- Pohlman, R. F. *et al.* Genetic and biochemical analysis of an endonuclease encoded by the IncN plasmid pKM101. *Nucleic Acids Res.* **21**, 4867–4872 (1993).
- Stuckey, J. A. & Dixon, J. E. Crystal structure of a phospholipase D family member. *Nature Struct. Biol.* **6**, 278–284 (1999).
- Leiros, I., Secundo, F., Zambonelli, C., Servi, S. & Hough, E. The first crystal structure of a phospholipase D. *Structure* **8**, 655–667 (2000).
- Gottlin, E. B., Rudolph, A. E., Zhao, Y., Matthews, H. R. & Dixon, J. E. Catalytic mechanism of the phospholipase D superfamily proceeds via a covalent phosphohistidine intermediate. *Proc. Natl Acad. Sci. USA* **95**, 9202–9207 (1998).
- Zhao, Y., Studkey, J. A., Lohse, D. L. & Dixon, J. E. Expression, characterization, and crystallization of a member of the novel phospholipase D family of phosphodiesterases. *Protein Sci.* **6**, 2655–2658 (1997).
- Raae, A. J., Kleppe, R. K. & Kleppe, K. Kinetics and effect of salts and polyamines on T4 polynucleotide ligase. *Eur. J. Biochem.* **60**, 437–443 (1975).
- Rotondo, G. & Frendewey, D. Purification and characterization of the Pac1 ribonuclease of *Schizosaccharomyces pombe*. *Nucleic Acids Res.* **24**, 2377–2386 (1996).
- Saito, K. *et al.* Specific association of Piwi with rasiRNAs derived from retrotransposon and heterochromatic regions in the *Drosophila* genome. *Genes Dev.* **20**, 2214–2222 (2006).
- Fukuhara, S. *et al.* Expression, purification, crystallization and preliminary X-ray crystallographic analysis of Zucchini from *Drosophila melanogaster*. *Acta Crystallogr. F.* (in the press).

Supplementary Information is available in the online version of the paper.

Acknowledgements We thank A. Kurabayashi, H. Kotani and Y. Tamaki for technical assistance; other members of the Siomi laboratory for discussions and comments on the manuscript; the beamline staff at BL32XU of SPring-8 for assistance in data collection; and T. Suzuki and H. Suga for technical suggestions and comments. This work was supported by a grant from the Japan Society for the Promotion of Science (JSPS) through its 'Funding Program for World-Leading Innovative R&D on Science and Technology (FIRST) program' to O.N., by the Core Research for Evolutional Science and Technology (CREST) program 'The Creation of Basic Medical Technologies to Clarify and Control the Mechanisms Underlying Chronic Inflammation' of the Japan Science and Technology Agency (JST) to O.N. and M.C.S., and by a Grant-in-Aid for Scientific Research from the Ministry of Education, Culture, Sports, Science and Technology (MEXT) of Japan to H.N., H.I., H.S., M.C.S. and O.N. K.S. is supported by the JSPS.

Author Contributions H.N., H.I., K.S., H.S., M.C.S. and O.N. conceived and designed the experiments and wrote the manuscript. H.N., S.F., L.B., N.M., T.N. and R.I. performed the structural analyses. H.I., K.S. and M.K.K. performed biochemical and biological analyses. K.N. and J.A. performed PLD activity assays. All authors discussed the data and the manuscript. M.C.S. and O.N. supervised all the work.

Author Information The atomic coordinates and structure factors are deposited in the Protein Data Bank under accession numbers 4GEL (DmZuc WT dimer), 4GEM (DmZuc K171A dimer) and 4GEN (DmZuc WT monomer). The authors declare no competing financial interests. Reprints and permissions information is available at www.nature.com/reprints. Readers are welcome to comment on the online version of the paper. Correspondence and requests for materials should be addressed to O.N. (nureki@biochem.s.u-tokyo.ac.jp) or M.C.S. (siomim@biochem.s.u-tokyo.ac.jp).

METHODS

Protein preparation. Protein samples were prepared as described²⁶. In brief, the gene encoding DmZuc (residues 41–253) was cloned between the *SacI* and *XhoI* sites of the pCold-GST vector²⁷. The protein was expressed at 20 °C in *E. coli* Rosetta 2 (DE3) (Novagen) and purified using glutathione-Sepharose (GE Healthcare). The protein was treated with Turbo3C protease (Nacalai Tesque) to remove the His₆-GST tag, and was further purified by NiNTA (Qiagen), Resource S (GE Healthcare) and Superdex 200 gel filtration (GE Healthcare). The DmZuc mutants were prepared using a PCR-based method, and the sequences were verified by DNA sequencing. The DmZuc mutants and MmZuc (residues 35–221) were prepared using a protocol similar to that used for WT DmZuc. DmZuc (residues 89–253) was expressed at 20 °C in *E. coli* Rosetta 2 (DE3) and purified using glutathione-Sepharose. The protein was treated with Turbo3C protease and was further purified by Superdex 75 gel filtration (GE Healthcare). SeMet-labelled DmZuc (residues 89–250) was expressed in *E. coli* B834 (DE3) (Novagen) and purified using a protocol similar to that used for the native protein.

Crystallization. During our expression trials, we found that DmZuc (residues 89–250) and the K171A mutant of DmZuc (residues 41–253) were more highly expressed than WT DmZuc (residues 41–253) in *E. coli*. Thus, we first solved the crystal structure of DmZuc (residues 89–250) by the MAD method, using a SeMet-labelled crystal. We next screened and optimized the crystallization conditions using the K171A mutant of DmZuc (residues 41–253). We then crystallized WT and K171A DmZuc under similar crystallization conditions, and solved the crystal structures by molecular replacement, using the structure of DmZuc (residues 89–250) as a search model.

Crystallization was performed at 20 °C by the vapour diffusion methods. Crystals of SeMet-labelled DmZuc (residues 89–250) were obtained by mixing 0.4 µl of protein solution (3 mg ml⁻¹ DmZuc, 10 mM Tris-HCl pH 8.0, 150 mM NaCl, 1 mM dithiothreitol (DTT)) and 0.4 µl of reservoir solution (50 mM MES pH 6.0, 8% polyethylene glycol 400, 100 mM KCl, 10 mM MgCl₂, 3% trehalose). Crystals of WT and K171A DmZuc (residues 41–253) were obtained by mixing 1 µl of protein solution (3–5 mg ml⁻¹ DmZuc, 10 mM Tris-HCl pH 8.0, 150 mM NaCl, 1 mM DTT) and 1 µl of reservoir solution (16% polyethylene glycol 3350, 200 mM KH₂PO₄).

Crystallography. X-ray diffraction data were collected at 100 K on beamline BL32XU at SPring-8 (Hyogo, Japan). The crystals were cryoprotected in reservoir solution supplemented with 30% ethylene glycol. Diffraction data were processed using HKL2000 (HKL Research Inc.). The structure of DmZuc (residues 89–250) was determined by the MAD method, using the 2.2-Å resolution data from the SeMet-labelled crystal. Four Se atoms were located using SHELXD²⁸, and the initial phases were calculated using SHARP²⁹, followed by automated model building using RESOLVE³⁰. The model was further built manually using COOT³¹ and refined using PHENIX³². The structures of WT and K171A DmZuc (residues 41–253) were solved by molecular replacement with MOLREP³³, using the structure of DmZuc (residues 89–250) as a search model. Data collection and refinement statistics are provided in Supplementary Table 1. Structural figures were prepared using CUEMOL (<http://www.cuemol.org>).

Nuclease assay. The RNA substrates used for nuclease assays were: 5'-AUU UAAUCAAGCUUAUCGAUACCGUCGACCUCGAGGGGGGGC-3' (42-nt), 5'-GGUCUGAUUUCGAUCUGGUUCCUGGAACAAAAGUGGCAG-3' (40-nt sense strand), 5'-CUGCCACUUUUGUCCAGGGAACAGAUUGAAUUA GACC-3' (40-nt antisense strand), and poly(U) (40-nt). ssRNAs were synthesized (Sigma) and labelled at their 5' ends using [γ -³²P]ATP and T4 polynucleotide kinase (New England Biolabs). For 3' end labelling, RNAs were labelled at their 3' ends using 5'-[³²P]pCp and T4 RNA ligase 1 (New England Biolabs). To make circular ssRNA, 5' end-labelled 42-nt RNAs were circularized by intramolecular ligation using T4 RNA ligase 1. The labelled RNAs were purified by electrophoresis on 12% denaturing polyacrylamide gels. To make dsRNA, 5' end-labelled 40-nt sense strand RNA and non-labelled 40-nt antisense strand RNA were mixed at a molar ratio of 1:2 (sense:antisense) in annealing buffer (10 mM Tris-HCl pH 7.5, 50 mM NaCl, 1 mM EDTA), heated at 95 °C for 15 min, and then cooled slowly to 30 °C.

³²P-end-labelled RNA substrate (10⁴ c.p.m.) was incubated with purified recombinant DmZuc (1.62 µM) in buffer A (25 mM HEPES-KOH pH 7.4, 2.5 mM EDTA, 5 mM DTT) for 1 h at 26 °C (37 °C for MmZuc). The reaction was terminated by treatment with proteinase K, followed by extraction with phenol-chloroform and precipitation with ethanol. The products were resolved on 20% denaturing polyacrylamide gels. The effects of NaCl on the nuclease activity were tested using the 42-nt ssRNA substrate in buffer B (25 mM HEPES-KOH pH 7.4, 5 mM magnesium acetate, 5 mM DTT, 0–100 mM NaCl). Terminator 5'-phosphate-dependent exonuclease was used in accordance with the manufacturer's instructions (Epicentre). The DNA substrate used for ssDNase

assays was 5'-AATTGGTACGTAGCGCTTGATCTAGAGGGGTTTGCCAAT AGCAATCCGACCGTTCCTCGTGCAGCAAT-3'.

PLD assay. PLD from *Actinomadura* sp. no. 362 was purchased from Meito Sangyo Inc. (Tokyo Japan). Tetraoleoyl cardiolipin (CL) (0.1 µmol; Avanti Polar Lipids) and dipalmitoyl phosphatidylcholine (PC) (0.5 µmol; Avanti Polar Lipids) were dried under nitrogen gas and resuspended in 10 mM HEPES pH 7.5 (0.6 ml) by sonication. The enzyme reaction was performed at 26 °C (DmZuc) or 37 °C (MmZuc and *Actinomadura* PLD) for 2 h with 10 µl of lipid solution, 38 µl of assay buffer (50 mM HEPES pH 7.5, 80 mM KCl, 3 mM MgCl₂, 2 mM CaCl₂, 1 mM DTT) and purified recombinant DmZuc (0.4 µg), MmZuc (0.4 µg) or *Actinomadura* PLD (0.3 U). The reaction was stopped by adding 450 µl of methanol containing an internal standard (1 µM diheptadecanoyl PC) and centrifuged at 21,500g. The sample solution (5 µl) was injected into liquid chromatography (LC) and analysed by tandem mass spectrometry (MS/MS). In brief, lipids were separated by Nanospace LC (Shiseido) with a silica column (5 µm, 2.0 mm × 150 mm; Shiseido), using a gradient of solvent A (5 mM ammonium formate in water) and solvent B (acetonitrile), and then analysed by MS/MS using a Quantum Ultra triple quadrupole mass spectrometer (Thermo Fisher Scientific). Lipids were monitored in negative-ion mode and quantified by multiple reaction monitoring (MRM). Tetraoleoyl CL, dioleoyl phosphatidic acid (PA), dipalmitoyl PA and dipalmitoyl PC were monitored with the MRM transition of *m/z* 1,456.1 > 281.2, *m/z* 699.4 > 281.2, *m/z* 759.5 > 255.2 and *m/z* 778.6 > 255.2, respectively. The ratio between analyte and internal standard peak area was used for quantification. Calibration curves (0.5–5,000 ng) and LC retention times for each compound were established using synthetic standards.

Rescue and dimerization assays in OSCs. The RNAi-resistant WT and mutants of DmZuc were prepared by a PCR-based method, using a pAc-Zuc-Myc vector¹⁵ as the template. Transfection was performed essentially as described previously¹⁰. In brief, trypsinized OSCs (5 × 10⁶ cells) were transfected with siRNA duplex (200 pmol), transferred to fresh OSC medium and incubated at 26 °C. Two days after transfection, OSCs (3 × 10⁶ cells) were again transfected with siRNA duplex (200 pmol) and plasmid vector (5 µg). The cells were again incubated at 26 °C for 2 days, and then total RNAs were purified using ISOGEN reagent (Nippon Gene). Total RNA (0.5 µg) was used to reverse transcribe target sequences using oligo(dT) primers. The resulting cDNAs were analysed by quantitative RT-PCR using a LightCycler real-time PCR system (Roche Diagnostics) and SYBR Premix Ex Taq (Takara). Relative steady-state mRNA levels were determined from the threshold cycle for amplification. Ribosomal protein 49 was used as an internal control. The expression levels of Piwi and DmZuc were analysed by western blotting using culture supernatants of anti-Piwi hybridoma cells (P4D2; 1:1 dilution)²⁵ and a mouse monoclonal antibody 9E10 against the Myc tag (1:1,000 dilution; Sigma), respectively.

Carboxy-terminal Flag-tagged DmZuc (pAc-Zuc-Flag) was prepared, by inserting oligonucleotides encoding a 3 × Flag tag between the *XhoI* and *BamHI* sites of pAc-Zuc-Myc (ref. 15). OSCs (5 × 10⁶ cells) were co-transfected with pAc-Zuc-Flag and either pAc-Zuc-Myc or pAcM-EGFP. Two days after transfection, the OSCs were homogenized in lysis buffer (30 mM HEPES pH 7.3, 150 mM potassium acetate, 2 mM magnesium acetate, 5 mM DTT, 0.1% Nonidet P40) to prepare OSC lysate. Zuc-Flag was immunoprecipitated using an anti-Flag M2 antibody (Sigma) immobilized on GammaBind beads (GE Healthcare). The mixtures were rocked at 4 °C for 2 h and the beads were washed five times with lysis buffer. After immunoprecipitation, proteins were resolved by SDS-PAGE and then detected by western blotting using anti-Flag M2 and anti-Myc antibodies.

RNA immunoprecipitation. C-terminal Myc-tagged, full-length DmZuc was expressed in OSCs by transfection. Two days after transfection, the OSCs were homogenized in lysis buffer (50 mM HEPES pH 7.5, 140 mM NaCl, 1 mM EDTA, 1 mM DTT, 2 µg ml⁻¹ pepstatin, 2 µg ml⁻¹ leupeptin, 0.5% aprotinin, 20 µl ml⁻¹ RNasin Plus (Promega), 1% Triton X-100) to prepare OSC lysate. Zuc-Myc was immunoprecipitated using a monoclonal anti-Myc antibody (9E10) immobilized on Dynabeads Protein G (Invitrogen). The mixtures were rocked at 4 °C for 2 h and the beads were washed five times with lysis buffer. Total RNAs were isolated from the immunoprecipitates with phenol-chloroform and were precipitated with ethanol. Total RNA was reverse transcribed using SuperScript III reverse transcriptase (Invitrogen) and a strand-specific RT primer for a fragment of the *flamenco* transcript. PCR was performed using Ex Taq DNA polymerase (Takara) and primers for a fragment of the *flamenco* transcript. The primer sequences were as follows: *flamenco* forward, 5'-AACGATGCTCAGTCCAG TGAA-3'; *flamenco* RT and reverse, 5'-AAAACCTTCTAGCTTGCCCTCT-3'.

27. Hayashi, K. & Kojima, C. pCold-GST vector: a novel cold-shock vector containing GST tag for soluble protein production. *Protein Expr. Purif.* **62**, 120–127 (2008).
28. Sheldrick, G. M. A short history of SHELX. *Acta Crystallogr. A* **64**, 112–122 (2008).
29. de La Fortelle, E. & Bricogne, G. SHARP: a maximum likelihood heavy-atom parameter refinement program for the MIR and MAD methods. *Methods Enzymol.* **276**, 472–494 (1997).

30. Terwilliger, T. C. & Berendzen, J. Automated MAD and MIR structure solution. *Acta Crystallogr. D* **55**, 849–861 (1999).
31. Emsley, P. & Cowtan, K. Coot: model-building tools for molecular graphics. *Acta Crystallogr. D* **60**, 2126–2132 (2004).
32. Adams, P. D. *et al.* PHENIX: building new software for automated crystallographic structure determination. *Acta Crystallogr. D* **58**, 1948–1954 (2002).
33. Vagin, A. & Teplyakov, A. Molecular replacement with MOLREP. *Acta Crystallogr. D* **66**, 22–25 (2010).